JOURNAL OF THE ROYAL SOCIETY Interface

FirstCite® e-publishing

J. R. Soc. Interface
doi:10.1098/rsif.2011.0508
Published online

Pressurized vascular systems for self-healing materials

A. R. Hamilton[1,2,†], N. R. Sottos[2,3,*] and S. R. White[2,4,*]

[1]*Department of Mechanical Science and Engineering, University of Illinois at Urbana-Champaign, 1206 West Green Street, Urbana, IL 61801, USA*
[2]*Beckman Institute for Advanced Science and Technology, 405 North Mathews Avenue, Urbana, IL 61801, USA*
[3]*Department of Materials Science and Engineering, University of Illinois at Urbana-Champaign, 1304 West Green Street, Urbana, IL 61801, USA*
[4]*Department of Aerospace Engineering, University of Illinois at Urbana-Champaign, 104 South Wright Street, Urbana, IL 61801, USA*

An emerging strategy for creating self-healing materials relies on embedded vascular networks of microchannels to transport reactive fluids to regions of damage. Here we investigate the use of active pumping for the pressurized delivery of a two-part healing system, allowing a small vascular system to deliver large volumes of healing agent. Different pumping strategies are explored to improve the mixing and subsequent polymerization of healing agents in the damage zone. Significant improvements in the number of healing cycles and in the overall healing efficiency are achieved compared with prior passive schemes that use only capillary forces for the delivery of healing agents. At the same time, the volume of the vascular system required to achieve this superior healing performance is significantly reduced. In the best case, nearly full recovery of fracture toughness is attained throughout 15 cycles of damage and healing, with a vascular network constituting just 0.1 vol% of the specimen.

Keywords: self-healing; microvascular; fracture; bioinspired

1. INTRODUCTION

Circulation in biological vascular systems enables the distribution of cells, hormones, oxygen, and nutrients, the removal of carbon dioxide and waste, and the maintenance of homeostasis. Fluid flow in these natural vascular systems is typically driven by a pressure gradient induced by the pumping action of a heart, even in primitive invertebrates such as earthworms [1]. In contrast, multi-cellular animals without circulatory systems (e.g. flatworms and jellyfish) rely on diffusion to transport nutrients and, as a result, are limited in size and complexity [2].

Synthetic vascularized materials have been created by a variety of manufacturing techniques with applications that include temperature regulation, damage-sensing and self-healing [3,4]. Self-healing materials possess the ability to heal in response to damage wherever and whenever it occurs in the material [5]. In polymers, self-healing has been demonstrated by three conceptual approaches: capsule-based healing systems, vascular healing systems and intrinsic reversible bonding [6]. Damage in vascular self-healing materials is repaired by the release of reactive fluids that subsequently polymerize to restore mechanical integrity. This approach has been applied to repair crack damage in coatings [7–9], at bimaterial interfaces [10,11], and within the vascularized material itself [12]. The most effective healing is achieved from two liquid-phase components (a resin and a hardener) that react upon contact [8]. The vascular system must therefore be capable of sequestering two reactive species within separate vascular networks until a damage event triggers their release. Most of the vascular self-healing materials reported to date use unpressurized networks, in which capillary forces draw the healing agents into damaged regions. Relying upon capillary flow limits the size of healable damage, since wicking is most effective when the length scales associated with the damage are less than the diameter of the vascular channels. Furthermore, unpressurized delivery of healing agents requires diffusional mixing—a relatively slow and highly localized process for typical resin–hardener systems—to occur for the healing reaction to initiate. In order to aid diffusion, a high volume fraction of interpenetrating vascular features is needed to reduce the distance over which the components must diffuse, but these dense networks can lead to diminished mechanical properties [13].

A biologically inspired solution to these problems with significant potential to improve the distribution and delivery of healing agents is the introduction of an actively controlled pumping system. Williams *et al.* [11] used external pumps to pressurize the flow of healing agents to regions of impact damage near the skin–core interface in a sandwich structure via a

*Authors for correspondence (n-sottos@illinois.edu; swhite@illinois.edu).
†Present address: Department of Mechanical and Manufacturing Engineering, Aalborg University, Fibigerstrade 16, 9220 Aalborg East, Denmark.

Received 28 July 2011
Accepted 8 September 2011

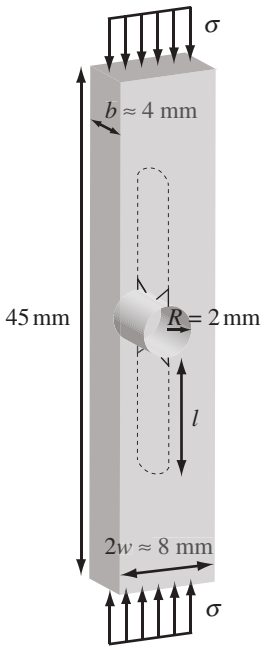

Figure 1. DCDC fracture sample geometry.

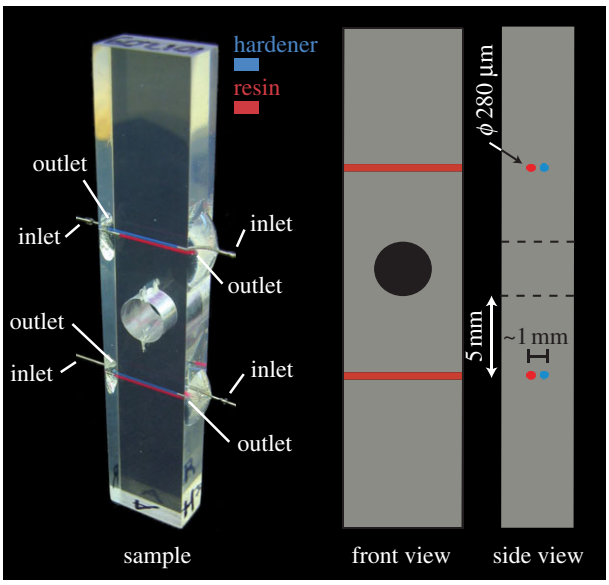

Figure 2. Image of a vascularized DCDC specimen, showing dispensing tips that served as healing agent inlets and outlets, and schematic detailing microchannel positions and contents.

network of silicone tubing embedded in the core material. The authors postulated that the highly pressurized flow of healing agents resulted in increased interaction of the flow fronts and improved mixing, but did not observe this directly. In this study, we explore the effect of actively controlled pressurization of vascular networks on the self-healing of internal damage in an epoxy matrix. To date, this type of damage in a vascular material has only been healed using relatively dense networks, in which capillary forces drive the flow of healing agents and diffusional mixing occurs within the damage volume [12]. Here, we employ external pumps to deliver healing agents via a sparse vascular network consisting of two isolated microchannels. Healing protocols are evaluated that use static pressurization to achieve steady flow rates into the damage volume, as well as dynamic pumping that results in out of phase, time-varying flow rates. Fluorescent dyes are used to visualize the distribution of each healing agent in the damage zone, and the healing performance of each pumping protocol is evaluated in terms of the fracture toughness recovered after each healing event.

2. MATERIAL AND METHODS

The double cleavage drilled compression (DCDC) fracture sample geometry (figure 1) was adopted to evaluate the recovery of fracture toughness after healing [12,14,15]. Upon application of a compressive load, transverse tensile stresses are induced at the crowns of the hole that drive the stable propagation of two self-similar, vertically oriented cracks. The epoxy matrix material consisted of a bisphenol A diglycidyl ether resin (Epon 828) cured with 40 pph aliphatic amidoamine hardener (Epikure 3274). Pairs of microchannels were positioned symmetrically on each half of the specimens (top and bottom), as shown in figure 2. The microchannels were molded using nylon fibres (230 μm in diameter), which were positioned across a silicone rubber mold at the desired locations. Specimens were cured for 24 h at room temperature followed by a 24 h post-cure at 30°C, after which the nylon fibres were removed—leaving straight, isolated microchannels, where the fibres had been extracted. Samples were polished flat to remove the meniscus on the open side of the mold, and precracks were initiated at the crowns of the hole. Precracking was accomplished by tapping a razor blade into a notch that had been scored on the crowns of the hole. Straight precracks were facilitated by applying a subcritical, compressive load to the sample during precracking.

On each half of the specimen, one microchannel was filled with a liquid resin (Epon 8132), while the other microchannel was filled with a liquid hardener (Epikure 3046). This particular two-part epoxy chemistry was used in previous demonstrations of vascular self-healing [8,9,12] due to the low viscosities of the components (Epon 8132 approx. 0.6 Pa s, Epikure 3046 approx. 0.2 Pa s) and the ability to cure at an equal (1 : 1) mix ratio (the stoichiometric ratio is 2.2 : 1). Pressurized reservoirs of the healing agents were connected to each microchannel via 1/16″ flexible PVC tubing and dispensing tips (EFD, Inc.) inserted 1–2 mm into each microchannel. The healing agent reservoirs were pressurized either with a static pressure head or using computer-controlled pumps. Microchannel outlets were closed during pumping, such that the only flow path for the healing agents after fracture was into the damage zone. Samples were compressed on a screw-driven load frame under displacement control at a rate of 2 μm s^{-1}. Images were captured at regular intervals, and crack lengths were measured optically. Loading was continued until the cracks had propagated within approximately 1–4 mm of the top/bottom of the sample. Samples were left on the load frame after fracture with a small compressive load maintained (approx. 50 N) to keep the sample stationary while healing agents were pumped into the crack.

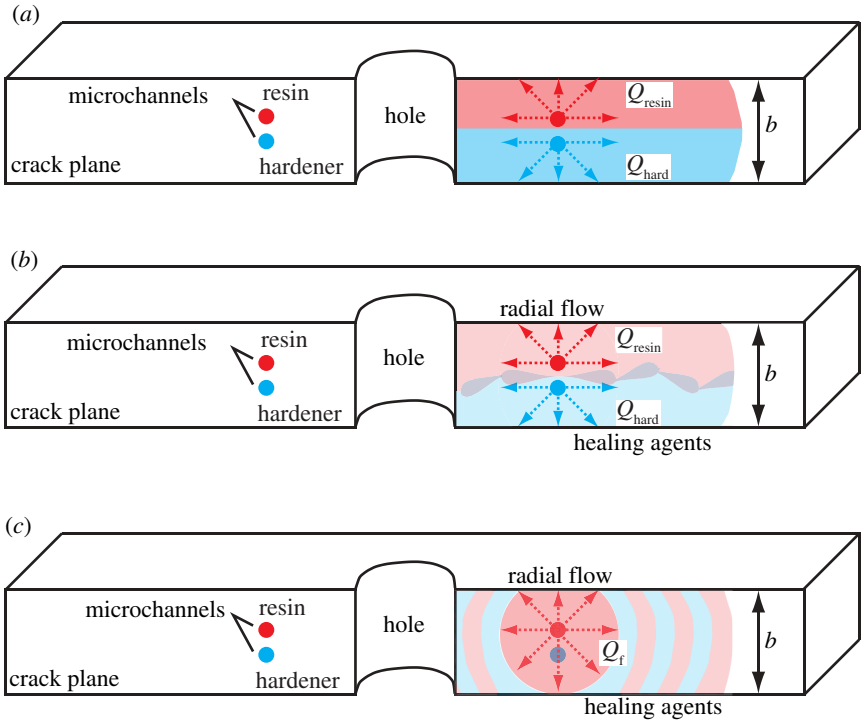

Figure 3. Expected distribution of healing agents in the crack plane as a result of (*a*) static pressure (*b*) dynamic pumping routine I and (*c*) dynamic pumping routine II.

The application of static pressure to healing agent reservoirs resulted in each healing agent flowing at constant, nearly equal rates into the damaged region. Based on the applied static heads of 965 mm and 330 mm for the resin and hardener, respectively, flow rates were estimated to range between 195 and 224 $\mu l\,h^{-1}$. The expected distribution of healing agents in the damage zone as a result of static pressure is illustrated in figure 3*a*. With crack separations of the order of several hundred microns, the flow of healing agents into the damage zone is laminar (Reynold's number $Re \sim 0.01-0.5$, with $Re > 2500$ necessary for turbulent flow). Consequently, minimal mixing is expected between the resin and hardener while infiltrating the damage zone [16]. The pumping protocols described in figure 4 were designed to improve mixing by perturbing the interface between the healing agents [17]. In dynamic pumping routine I, shown in figure 4*a*, punctuated bursts of hardener were injected into a steady flow of resin to increase the contact area between the two healing agents, as illustrated in figure 3*b*. Each cycle of pumping routine I consisted of a period in which the bursts of hardener were short (0.3 s long) and infrequent (every 12 s), followed by a period when the bursts were longer (1 s long) and more frequent (every 5 s). The varying length and frequency of hardener bursts were determined empirically to induce longer wavelength perturbations to the resin–hardener interface (i.e. folding). Dynamic pumping routine II, depicted in figure 4*b*, was designed to maximize the contact area between the two healing agents in the crack plane by alternating between pumping only the resin and pumping only the hardener. The volume of healing agent pumped during each period was calculated to cover the entire thickness of the sample (assuming radial flow from the microchannel) according to

$$v_f = Q_f t_f \geq \frac{\pi}{4} b^2 \delta, \tag{2.1}$$

where v_f is the volume of fluid pumped, Q_f is the volumetric flow rate of the fluid (either Q_{resin} or Q_{hard} in figure 4), t_f is the period of time over which the fluid is pumped (either t_{resin} or t_{hard} in figure 4), b is the sample thickness and δ is the crack separation near the microchannels. The intended result of each pumping strategy is illustrated in figure 3.

Static pumping was stopped as soon as the damage volume had been filled with healing agents. Dynamic pumping routines were continued beyond the time required to fill the damage volume for a total of 20 repetitions of the cycles shown in figure 4, resulting in total pumping times of 2000 s, and 1800 s for routines I and II, respectively. Excess healing agents that flowed out of the damage zone onto the surface of the specimens were removed by wiping the fluid to the base of the sample with a non-absorbent material (to avoid wicking, which might have influenced the fluid flow).

After each pumping protocol was complete, samples were disconnected from the supply of healing agents and placed into an oven at 30°C for 48 h to heal. These modest curing conditions accelerated the reaction of healing agents and expedited testing of the healed samples [8], but were not required for the healing agents to react. Microchannel outlets were opened during the healing cycle to allow the flow of the healing agents through the microchannels, driven by a small pressure head (estimated flow of 2–6 $\mu l\,h^{-1}$ based on a static head of approx. 10 mm) in order to prevent healed material from forming in the microchannel and

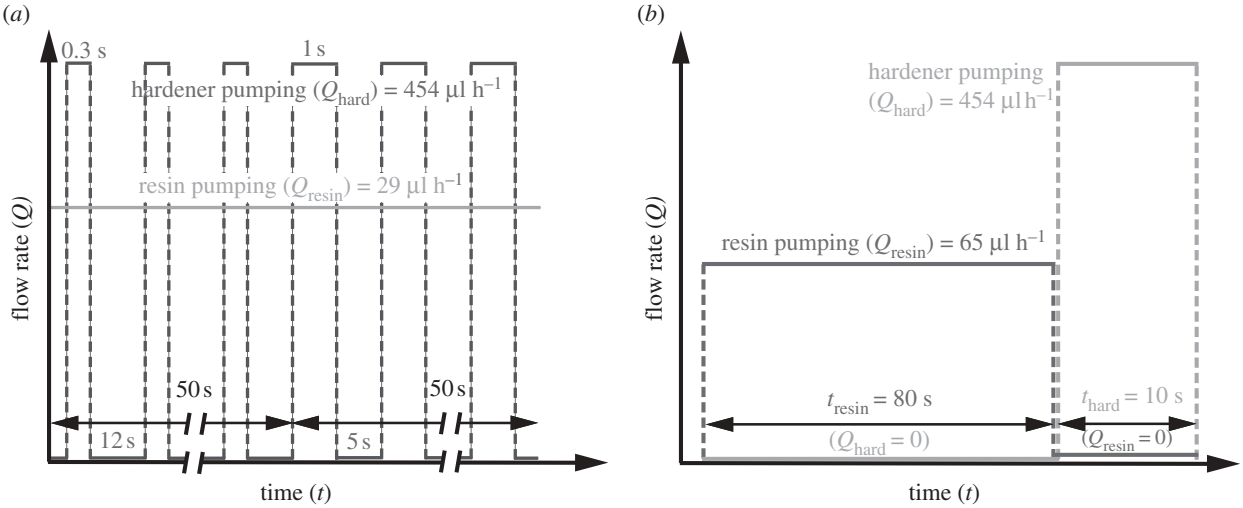

Figure 4. Plots of the healing agent flow rates in dynamic pumping (*a*) routine I and (*b*) routine II.

sealing off access to the crack plane. Samples denoted as 'clamped' had a 100 µm thick piece of aluminium shim stock placed in the precrack region near the hole, and a crack-closing force of 17–19 N applied laterally during healing so that the thickness of the healed material was controlled.

Healed samples were fractured following the same experimental protocol as with virgin samples, except in cases when the healed fracture toughness exceeded the virgin fracture toughness. In these cases, compressive loading was discontinued to avoid catastrophic sample failure, and fracture was induced by wedge loading with a razor blade so that further healing cycles could be conducted.

3. RESULTS AND DISCUSSION

3.1. Fracture testing

Representative crack growth data for a plain epoxy DCDC sample are shown as a function of applied stress in figure 5*a*. An analytical model based on linear elastic fracture mechanics coupled with simple beam theory [14] predicts a stress intensity factor (K) that is independent of crack length after sufficient crack extension away from the hole:

$$K = A\sigma, \tag{3.1}$$

where σ is the applied compressive stress and A is a function of the sample dimensions ($2w$ and R):

$$A = \frac{2}{\sqrt{wR}}\left(\frac{3 + 2\ln(w/R)}{4(w/R)} - \frac{1}{4(w/R)^3}\right). \tag{3.2}$$

The crack length independence of K, combined with the homogeneous mechanical properties (i.e. constant K_{IC}) of the epoxy matrix, results in a constant applied stress for crack propagation, exhibited in figure 5*a*) at longer crack lengths ($l/R \gtrsim 1$) and denoted with a dashed line.

Crack propagation in vascularized samples (figure 5*b*) is similar to that in plain samples until the cracks intersect the microchannels ($l/R = 2.5$). The microchannels temporarily arrest crack growth, resulting in a higher stress for propagation in the material at this location. When crack growth resumes, the propagation is typically unstable (hence no data points were collected after the microchannel location), but the cracks arrest before complete cleavage of the sample. The applied stress used in equation (3.2) to calculate the fracture toughness of virgin vascular specimens is the maximum stress, as indicated by the horizontal dashed line in figure 5*b*. Using the maximum stress accounts for toughening due to the crack arrest at the microchannels and provides a conservative estimate of healing efficiency. Average values of virgin fracture toughness are given for each type of specimen in table 1.

Crack propagation in healed samples either resembles that of neat samples (i.e. constant applied stress for crack propagation), or displays an increasing level of stress for continued crack propagation. The latter behaviour was reported previously and is associated with non-uniform curing of the healing agents in the crack plane [12]. As with virgin fracture, the maximum stress, designated by the dashed horizontal lines in figure 5*c*, was used to calculate the fracture toughness of healed specimens.

3.2. Healing agent delivery

The flow of healing agents into the damage volume, after the virgin fracture event, was observed using fluorescent-dyed healing agents, but subsequent delivery was obscured by the presence of fluorescent-healed material from previous healing events. The final distribution of healing agents in the crack plane resulting from constant flow under static pressure and the two dynamic pumping protocols are compared in figure 6. As expected, constant flow under static pressure results in a single interface between the resin and hardener that spans the length of the crack (figure 6*a*). Dynamic pumping using routine I produces a distribution of healing agents similar to flow under static pressure. The fluorescent images show no clear evidence of enhanced mixing at the resin–hardener interface due to the pulsatory flow of pumping routine

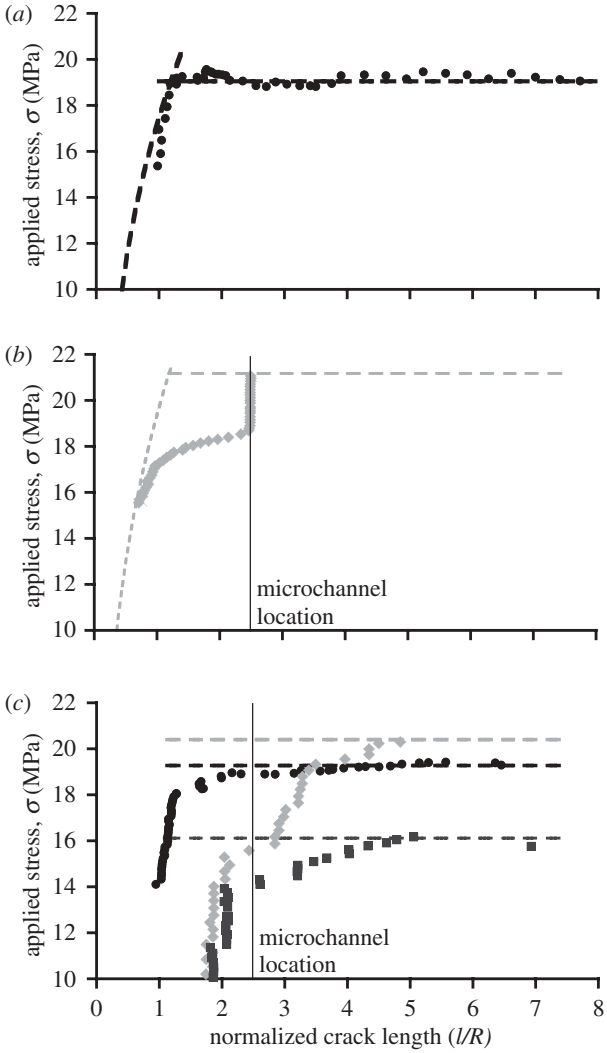

Figure 5. Applied compressive stress as a function of normalized crack length for representative (*a*) plain epoxy (*b*) virgin vascular and (*c*) healed vascular specimens. Dashed lines indicate model predictions; the stress level indicated by the horizontal dashed lines was used in equation (3.2) to calculate K_{IC}. Circles, healing cycle 1; diamonds, healing cycle 7; squares, healing cycle 15.

I; however the continued infusion of healing agents after complete infiltration of the damage volume resulted in folding of the interface, as healing agents already present in the damage zone were displaced to accommodate the excess healing agents supplied by the microchannels. This folding is shown in figure 6*b* above the microchannels, where striations span the crack through the thickness of the sample. More of these through-thickness striations are present in figure 6*c* after the application of pumping routine II, which was developed specifically to enhance interface folding.

The progression of healing agents in the course of infusion using pumping routine II is shown in figure 7. The crack spans the entire field of view in each frame, but is indiscernible in the images until it was filled with the dyed healing agents. The entire damage volume was nearly filled after 135 s (in the course of the second pumping cycle); however continued pumping led to the formation of well-mixed regions above and below the microchannels. As with pumping routine I,

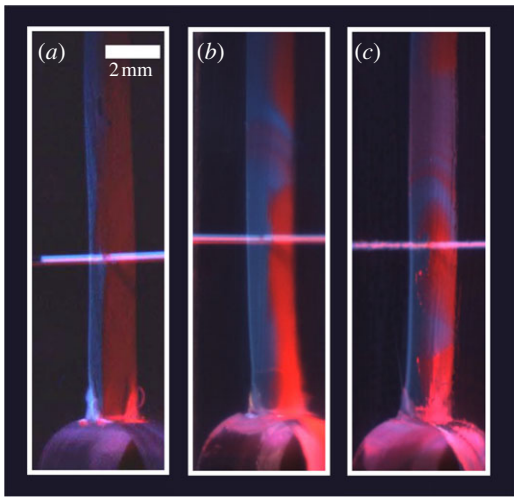

Figure 6. Final distribution of healing agents (resin in red, hardener in blue) in the crack plane after (*a*) constant flow under static pressure, (*b*) dynamic pumping routine I, and (*c*) routine II.

Table 1. Average value of virgin fracture toughness within 1 s.d. and number of specimens (n) for each specimen type.

sample type	$(K_{IC})_{virgin}$ (MPa m$^{1/2}$)	n
plain epoxy	0.64 ± 0.02	6
static pressure	0.73 ± 0.02	3
dynamic pumping routine I	0.71 ± 0.05	4
dynamic pumping routine II (unclamped)	0.65 ± 0.03	4
dynamic pumping routine II (clamped)	0.65 ± 0.05	4

the excess volume of healing agents pumped into the damage zone was accommodated by the displacement of healing agents onto the surface of the specimen. Under the action of pumping routine II, a single fold in the resin–hardener interface is formed by each pumping cycle (for a total of 20), but the folds become compressed and obscured as subsequent pumping forced the striations away from the microchannels and farther along the length of the crack.

3.3. Recovery of fracture toughness

The healing efficiency (η) is defined as the ratio of the healed sample fracture toughness to the virgin fracture toughness [5,18]. For the DCDC specimen geometry, this reduces to

$$\eta = \frac{(K_{IC})_{healed}}{(K_{IC})_{virgin}} \times 100 = \frac{(\sigma_P)_{healed}}{(\sigma_P)_{healed}} \times 100. \qquad (3.3)$$

Healing efficiencies are presented in figure 8 for each pumping protocol as a function of the number of cycles of fracture and healing. Flow under constant pressure resulted in a consistent recovery of approximately 58 per cent of the virgin fracture toughness, which was largely independent of healing cycle. The increased degree of mixing resulting from the dynamic pumping

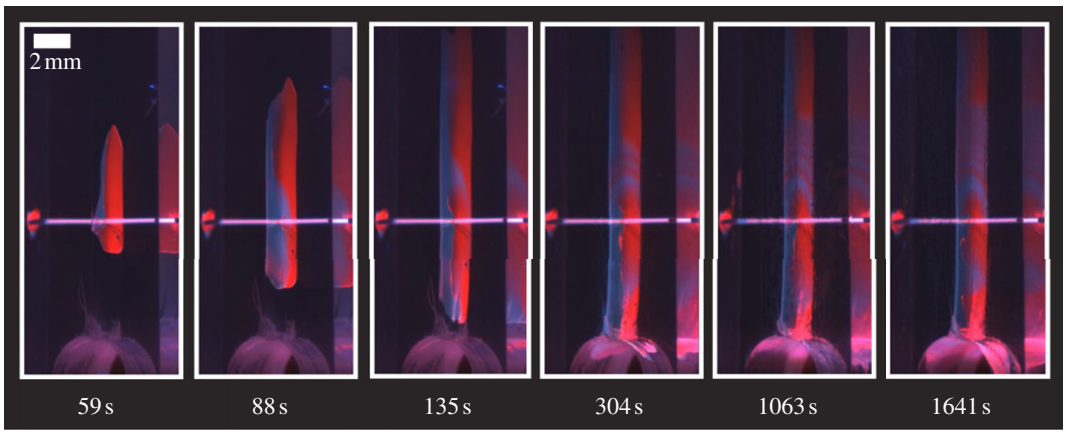

Figure 7. Fluorescent images of resin (red) and hardener (blue) healing agents infiltrating a fractured specimen during pumping routine II. The time elapsed from the start of pumping is denoted under each image frame.

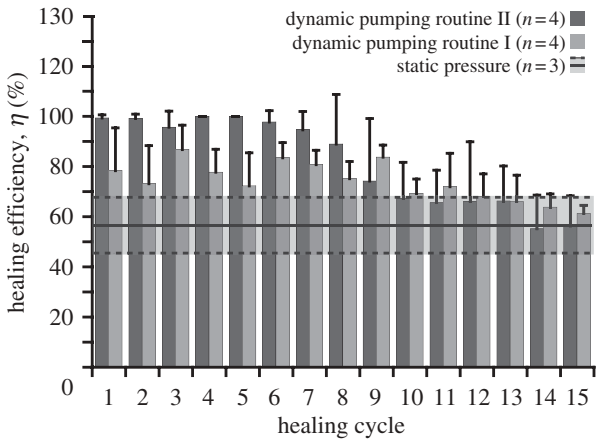

Figure 8. Average healing efficiencies for samples subjected to each type of pumping protocol. Error bars and dashed lines bound 1 s.d. and the number of samples tested for each data point (n) is indicated in the key.

protocols translated into consistently higher healing efficiencies when compared with constant pressure. Pumping routine I produced a maximum healing efficiency of 87 per cent, while pumping routine II produced healing efficiencies of nearly 100 per cent for the first seven cycles. After 15 healing cycles, testing was discontinued, with all of the samples still actively healing and presumably capable of undergoing further recovery. In cases when a healed sample did not fracture at or below the virgin fracture load, the test was halted (as described in §2) and a healing efficiency of 100 per cent was used to compute the average. Healed fracture toughnesses exceeding the virgin fracture toughness are possible because the sample geometry has a preferred crack path that prevents crack deflection.

The superior healing performance in the first eight healing cycles of samples healed using pumping routine II is attributed to the higher degree of mixing observed in these samples. Top views of the healed film are shown in figure 9 for samples healed using pumping routine II. After one healing cycle (figure 9*a*), the regions where healed agents polymerized correspond to the location of alternating resin–hardener striations in figure 6*c*. After 15 cycles of damage and healing, the healed material spans the entire fracture surface (figure 9*b*). The intermediate performance of the samples healed using pumping routine I is likely due to the formation of fewer healing agent interfaces in the crack plane (as shown in figure 6). The perturbation of the resin–hardener interface by the pulsatory flow of hardener may have promoted enhanced mixing along the resin–hardener interface that spans the length of the crack, and thereby account for the improved healing performance over the samples with constant flow, along with the limited folding and striations formed. The healing efficiencies of both the dynamic pumping protocols degraded after about eight or nine healing cycles, reaching levels comparable with those of the constant flow samples by the end of testing.

3.4. Effect of healed film accumulation

Over the course of multiple cycles of damage and healing, a thick film of healed material accumulated between the crack faces of the dynamically pumped samples. The change of the sample width ($2w$) measured at the centre of the sample is plotted as a proxy for the total thickness of the healed material in the crack plane (δ) in figure 10, along with the healing efficiencies of samples pumped using routine II. The healed material thickness was approximately 600–700 μm when the healing efficiencies started to decline (after eight cycles of healing), compared with an initial thickness of about 100 μm after the first healing event. This degradation of healing performance is attributed to the accumulation of excess healed material in the damage zone that impedes the flow of healing agents.

The data denoted as clamped in figure 10 correspond to samples that were laterally clamped during the healing cure cycle to suppress the thickness of the healed material by bringing the crack faces into closer contact during healing. The healing performance of the clamped and unclamped samples were similar up to the nineth healing cycle, at which point the healing efficiencies of the unclamped samples started to decline, while that of the clamped samples persisted at higher levels for the duration of testing. The maximum healed film thickness of the clamped samples in figure 10 (approx. 300 μm) never reached the thicknesses of the unclamped samples that

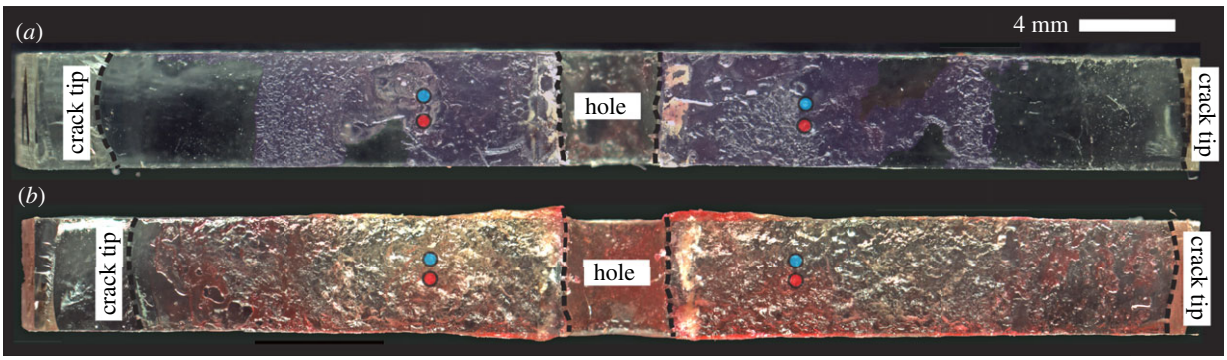

Figure 9. Images of fracture surfaces after (*a*) a single cycle of damage and healing and (*b*) 15 healing cycles. Microchannel locations are denoted with coloured circles and the healed film location in (*a*) is highlighted with false colour (purple).

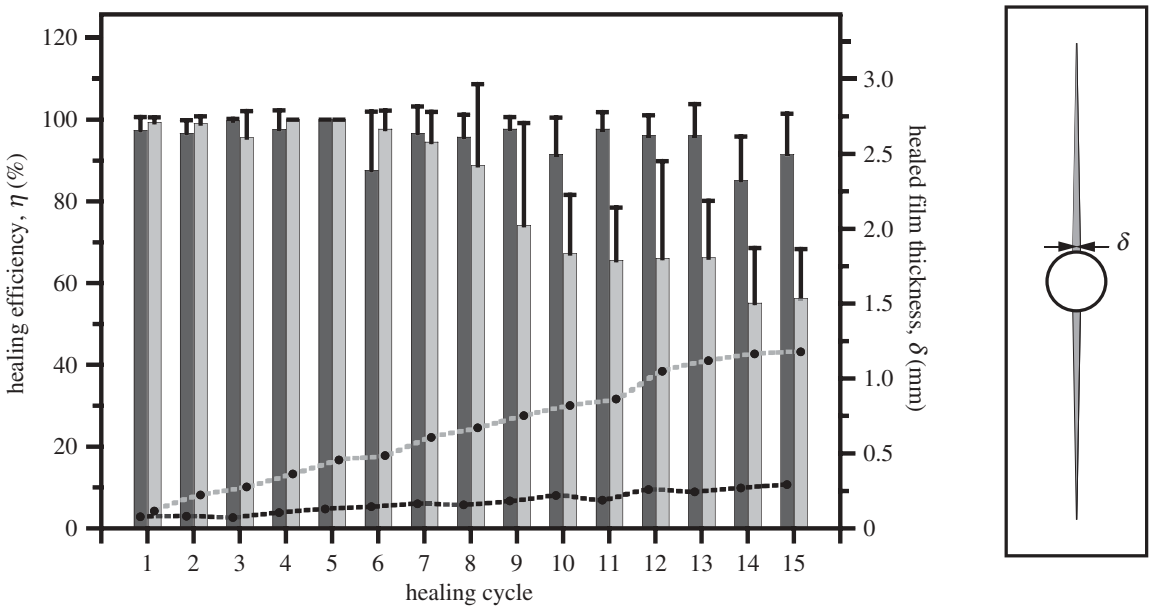

Figure 10. Healing efficiency (clamped, black bars ($n = 4$); unclamped, grey bars ($n = 4$)) and healed film thickness (clamped, black dashed lines with dots; unclamped, grey dashed lines with dots) of samples undergoing dynamic pumping routine II with and without lateral clamps applied during healing. Error bars and dashed lines bound 1 s.d. and the number of samples tested for each data point (n) is indicated in the legend. Schematic illustrates the location where healed film thickness was measured.

corresponds to diminishing healing efficiency (approx. 600 μm), suggesting that a critical thickness is necessary to interfere with healing agent flow and subsequent healing.

3.5. Comparison with capillary flow of healing agents

Although the upper limit of healable damage volume was not explored, active pumping and reservoirs of healing agents remove the constraints of limited healing agent supply and the reliance upon capillary forces to drive flow. With a total microchannel volume of about 1.3 μl, the vascular specimens in this study healed damage volumes of approximately 7.4 μl (assuming a crack separation equal to the 100 μm shim stock used with the clamped samples) or more. Therefore, complete infiltration of the damage volume was only possible with an external supply of healing agents. The small vascular system volume fraction of 0.1% was sufficient for effective healing in part because the well-defined locations of crack initiation and propagation facilitated effective microchannel placement, but also because pumping the healing agents improved the degree of mixing in the damage volume. In figure 11, the healing efficiencies resulting from the best case of dynamic pumping (protocol II, clamped) and static pressurization are compared with previous results in which vascular systems consisting of 80 microchannels and a total volume of more than 20.1 μl (a volume fraction of over 1.4%) were implemented for healing, capillary forces induced healing agent flow, and mixing relied upon diffusion [12]. The superior healing performance of the dynamically pumped sample is evident. Interestingly, even the samples with static pumping outperformed the unpressurized samples after the first healing cycle.

In addition to improving the degree of mechanical recovery, the repeatability of the self-healing response was extended from six to 13 cycles of damage in the case of unpressurized samples [12], to 15 cycles and

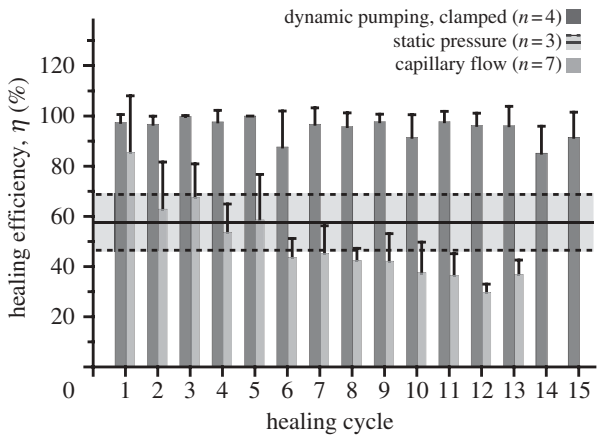

Figure 11. Comparison of average healing performances for samples healed using pumping routine II, static pressure, and capillary flow [12]. Error bars and dashed lines bound 1 s.d. and the number of samples tested for each data point (n) is indicated in the key.

beyond with pressurized healing agent delivery and a small static pressure applied during healing. This prolonged healing ability can be attributed to the continuous flow of healing agents preventing blockages in and around the microchannels, and to the stronger driving force for healing agent delivery to the damage zone afforded by pumping.

Although the results of active pumping are promising, challenges to the implementation of this pressurized vascular self-healing motif in practical applications remain. Replicating the laboratory protocols described here in a fully autonomous material requires damage-sensing to start and stop the pumping protocols. One simple means of triggering pumping is by monitoring the fluid pressure in the vasculature to detect ruptures [19,20]. Another challenge is preventing the continuous loss of healing agents after mechanical damage ruptures the vascular system, perhaps by developing a strategy for sealing the vascular system after the release of healing agent. Finally, the dynamic pumping routines in this work were developed for a specific damage volume size and shape, which may not be known *a priori* in parts with a complex geometry, varying service loads, or multiple failure modes. Simulations of these mixing strategies could help identify the factors influencing mixing and aid in further optimization [21,22].

4. CONCLUSION

High healing efficiencies were achieved using a simple vascular system consisting of two parallel microchannels to deliver reactive fluids to a region of internal damage. With external reservoirs of healing agents, a damage volume larger than the total vascular volume was effectively filled and healed. Employing pressure-driven flow removes the reliance upon capillary forces and, in the cases of dynamic pumping, mixing of the two healing agents in the damaged region was enhanced. Improved mixing resulted in the formation of consistently tougher healed material over the course of numerous damage–heal cycles when compared with the alternative strategy of employing a dense spatial distribution of vascular features to achieve mixing via diffusion alone, resulting in inferior mechanical recovery.

This work was supported by the Air Force Office of Scientific Research Multi-disciplinary University Research Initiative (grant no. F49550-05-1-0346). The authors thank their colleagues in the Autonomous Materials Systems Research group at the Beckman Institute for Advanced Science and Technology, especially Dr Solar Olugebefola and John Fettig for their input on pumping strategies.

REFERENCES

1 Noordergraaf, A. 1978 *Circulatory system dynamics*. New York, NY: Academic Press.
2 Schmidt-Rhaesa, A. 2007 *The evolution of organ systems*. Oxford, UK: Oxford University Press.
3 Olugebefola, S. C. *et al.* 2010 Polymer microvascular network composites. *J. Comp. Mater.* **44**, 2587–2603. (doi:10.1177/0021998310371537)
4 Trask, R. S. & Bond, I. P. 2009 Bioinspired engineering study of Plantae vascules for self-healing composite structures. *J. R. Soc. Interface* **7**, 921–993. (doi:10.1098/rsif.2009.0420)
5 White, S. R., Sottos, N. R., Geubelle, P. H., Moore, J. S., Kessler, M. R., Sriram, S. R., Brown, E. N. & Viswanathan, S. 2001 Autonomic healing of polymer composites. *Nature* **409**, 794–797. (doi:10.1038/35057232)
6 Blaiszik, B. J., Kramer, S. L. B., Olugebefola, S. C., Moore, J. S., Sottos, N. R. & White, S. R. 2010 Self-healing polymers and composites. *Annu. Rev. Mater. Res.* **40**, 179–211. (doi:10.1146/annurev-matsci-070909-104532)
7 Toohey, K. S., Sottos, N. R., Lewis, J. A., Moore, J. S. & White, S. R. 2007 Self-healing materials with microvascular networks. *Nat. Mater.* **6**, 581–585. (doi:10.1038/nmat863)
8 Toohey, K. S., Hansen, C. J., Lewis, J. A., White, S. R. & Sottos, N. R. 2009 Delivery of two-part self-healing chemistry via microvascular networks. *Adv. Func. Mater.* **19**, 1399–1405. (doi:10.1002/adfm.200801824)
9 Hansen, C. J., Wu, W., Toohey, K. S., Sottos, N. R., White, S. R. & Lewis, J. A. 2009 Self-healing materials with interpenetrating microvascular networks. *Adv. Mater.* **21**, 1–5. (doi:10.1002/adma.200900588)
10 Williams, H. R., Trask, R. S. & Bond, I. P. 2007 Self-healing composite sandwich structures. *Smart Mater. Struct.* **16**, 1198–1207. (doi:10.1088/0964-1726/16/4/031)
11 Williams, H. R., Trask, R. S. & Bond, I. P. 2008 Self-healing sandwich panels: restoration of compressive strength after impact. *Comp. Sci. Tech.* **68**, 3171–3177. (doi:10.1016/j.compscitech.2008.07.016)
12 Hamilton, A. R., Sottos, N. R. & White, S. R. 2010 Self-healing of internal damage in synthetic vascular materials. *Adv. Mater.* **22**, 5159–5163. (doi:10.1002/adma.201002561)
13 Hamilton, A. R., Sottos, N. R. & White, S. R. 2010 Local strain concentrations in a microvascular network. *Exp. Mech.* **50**, 255–263. (doi:10.1007/s11340-009-9299-5)
14 Plaisted, T. A., Amirkhizi, A. V. & Nemat-Nasser, S. 2006 Compression-induced axial crack propagation in DCDC polymer samples: experiments and modeling. *Int. J. Fract.* **141**, 447–457. (doi:10.1007/s10704-006-9006-9)
15 Plaisted, T. A. & Nemat-Nasser, S. 2007 Quantitative evaluation of fracture, healing and re-healing of a

reversibly cross-linked polymer. *Acta Mater.* **55**, 5684–5696. (doi:10.1016/j.actamat.2007.06.019)

16 Stroock, A. D., Dertinger, S. K. W., Ajdari, A., Mezic, I., Stone, H. A. & Whitesides, G. 2002 Chaotic mixer for microchannels. *Science* **295**, 647–651. (doi:10.1126/science.1066238)

17 Sun, C.-L. & Sie, Y. 2010 Active mixing in diverging microchannels. *Microfluidics Nanofluidics* **8**, 485–495. (doi:10.1007/s10404-009-0478-6)

18 Brown, E. N., White, S. R. & Sottos, N. R. 2002 Fracture testing of a self-healing polymer composite. *Exp. Mech.* **42**, 372–379. (doi:10.1007/BF02412141)

19 Kousourakis, A., Mouritz, A. & Bannister, M. 2006 Interlaminar properties of polymer laminates containing internal sensor cavities. *Comp. Struct.* **75**, 610–618. (doi:10.1016/j.compstruct.2006.04.086)

20 Kousourakis, A., Bannister, M. K. & Mouritz, A. P. 2008 Tensile and compressive properties of polymer laminates containing internal sensor cavities. *Compos. A* **39**, 1394–1403. (doi:10.1016/j.compositesa.2008.05.003)

21 Fu, L.-M. & Chien-Hsiung, T. 2007 Design of interactively time-pulsed microfluidic mixers in microchips using numerical simulation. *Jpn. J. Appl. Phys.* **46**, 420–429. (doi:10.1143/JJAP.46.420)

22 Shuo, H., Yang, L. & Xu, Y. S. 2010 Effect of viscosities on mixing in a patterned micro mixer. *Commun. Theor. Phys.* **53**, 952–956. (doi:10.1088/0253-6102/53/5/31)